RESEARCH ARTICLE

Common and unique connectivity at the interface of motor, neuropsychiatric, and cognitive symptoms in Parkinson's disease: A commonality analysis

Stefan Lang[1,2,3] | Zahinoor Ismail[1,2,3,4,5] | Mekale Kibreab[1,2,3] | Iris Kathol[1,2,3] | Justyna Sarna[1,2,3] | Oury Monchi[1,2,3,6]

[1]Cumming School of Medicine, University of Calgary, Calgary, Alberta, Canada

[2]Department of Clinical Neurosciences, University of Calgary, Calgary, Alberta, Canada

[3]Hotchkiss Brain Institute, University of Calgary, Calgary, Alberta, Canada

[4]Department of Psychiatry, University of Calgary, Calgary, Alberta, Canada

[5]Mathison Center for Brain and Mental Health Research, University of Calgary, Calgary, Alberta, Canada

[6]Department of Radiology, University of Calgary, Calgary, Alberta, Canada

Correspondence
Oury Monchi, 3330 Hospital Drive NW, Calgary, AB T2N 4N1, Canada.
Email: oury.monchi@ucalgary.ca

Abstract

Parkinson's disease (PD) is characterized by overlapping motor, neuropsychiatric, and cognitive symptoms. Worse performance in one domain is associated with worse performance in the other domains. Commonality analysis (CA) is a method of variance partitioning in multiple regression, used to separate the specific and common influence of collinear predictors. We apply, for the first time, CA to the functional connectome to investigate the unique and common neural connectivity underlying the interface of the symptom domains in 74 non-demented PD subjects. Edges were modeled as a function of global motor, cognitive, and neuropsychiatric scores. CA was performed, yielding measures of the unique and common contribution of the symptom domains. Bootstrap confidence intervals were used to determine the precision of the estimates and to directly compare each commonality coefficient. The overall model identified a network with the caudate nucleus as a hub. Neuropsychiatric impairment accounted for connectivity in the caudate-dorsal anterior cingulate and caudate-right dorsolateral prefrontal-right inferior parietal circuits, while caudate-medial prefrontal connectivity reflected a unique effect of both neuropsychiatric and cognitive impairment. Caudate-precuneus connectivity was explained by both unique and shared influence of neuropsychiatric and cognitive symptoms. Lastly, posterior cortical connectivity reflected an interplay of the unique and common effects of each symptom domain. We show that CA can determine the amount of variance in the connectome that is unique and shared amongst motor, neuropsychiatric, and cognitive symptoms in PD, thereby improving our ability to interpret the data while gaining novel insight into networks at the interface of these symptom domains.

KEYWORDS

cognition, commonality analysis, connectivity, mild behavioral impairment, motor, Parkinson's disease, resting state

---

1 | INTRODUCTION

Parkinson's disease (PD) is a neurodegenerative disorder characterized by a classic set of motor symptoms, including tremor, rigidity, bradykinesia, and postural instability (Jankovic, 2008). However, it is now evident that many non-motor symptoms arise early in the course of the disease and significantly impact quality of life (Poewe, 2008; Schapira, Chaudhuri, & Jenner, 2017). These non-motor symptoms include cognitive and neuropsychiatric impairment. Cognitive symptoms include impairments of executive function, attention, memory, language, and visuospatial abilities (Janvin, Larsen, Aarsland, & Hugdahl, 2006; Svenningsson, Westman, Ballard, & Aarsland, 2012; Williams-Gray et al., 2009; Yarnall et al., 2014). Neuropsychiatric symptoms include depression, anxiety, apathy, impulse control disorders, and perceptual distortions (Aarsland, Marsh, & Schrag, 2009; Castrioto, Thobois, Carnicella, Maillet, & Krack, 2016; Kulisevsky et al., 2008). PD can therefore be understood as a multi-system disorder, with three main symptom domains: motor, neuropsychiatric, and cognitive. While each of these domains is independent to some degree, they are also correlated amongst each other. For example, worse cognitive performance is associated with more severe motor (Burn, Rowan, Allan, Molloy, & Mckeith, 2006; Hu et al., 2014; Schneider, Sendek, & Yang, 2015) and neuropsychiatric symptoms (Aarsland, Taylor, & Weintraub, 2014; Monastero, Di Fiore, Ventimiglia, Camarda, & Camarda, 2013; Yoon et al., 2019). Similarly, worse neuropsychiatric symptoms can be associated with higher motor severity (Burn et al., 2012; Lee & Koh, 2015; Riedel et al., 2010; Solla et al., 2011). The neural representation of each of these symptom spheres has been investigated individually, often while controlling for the influence of one or the other domains. These changes have been summarized in previous review articles (Biundo, Weis, & Antonini, 2016; Filippi, Sarasso, & Agosta, 2019; Gao & Wu, 2016; Prodoehl, Burciu, & Vaillancourt, 2014; Tahmasian et al., 2017; Valli, Mihaescu, & Strafella, 2019; Wen, Chan, Tan, & Tan, 2016) and consist of diverse, heterogenous changes throughout the brain. However, while understanding the separate neural representations of each symptom domain is useful, it may be equally interesting to gain insight into neural features which may lie at the interface between the domains. This concept is visualized in Figure 1. Here, we conceptualize the entire neural network involved in PD as the PD-Network. Hypothetically, within this PD-Network, there are networks involved in neuropsychiatric, cognitive, and motor symptoms, with a subnetwork situated at the interface of the domains. This subnetwork may be further decomposed into connections which are unique (U1, U2, U3) and common (C1, C2, C3, C4) to each symptom sphere.

Commonality analysis (CA) is a method of detailed variance partitioning in multiple regression, used to decompose the coefficient of determination (R^2) into unique and common variance of each predictor in the model (Nimon & Reio, 2011; Prunier, Colyn, Legendre, Nimon, & Flamand, 2015; Ray-Mukherjee et al., 2014; Zientek & Thompson, 2006). These unique and common variance partitions, known as commonality coefficients, represent nonoverlapping components of variance which always sum to R^2 and can be viewed as effect
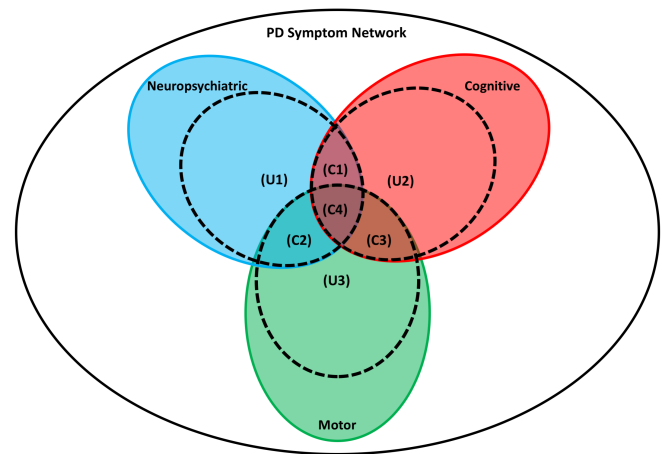
FIGURE 1 Three distinct but overlapping symptoms (neuropsychiatric, cognition, motor) spheres in PD. At the interface of these domains, there may exist a subset of connections which can be explained through a combination of unique (U1, U2, U3) and shared (C1, C2, C3, C4) contributions from each symptom domain

sizes (<1% negligible, >1% small, >9% moderate, and > 25% large) (Marchetti, Loeys, Alloy, & Koster, 2016). When divided by R^2, one can determine the relative contribution of each partition to the total explained variance. Considering a model with three predictors (x1, x2, x3), the total variance is explained with seven commonality coefficients. Using Figure 1 as an example, the unique contribution of neuropsychiatric symptoms is specified as U1, while the common contribution of neuropsychiatric and cognitive impairment is C2, and so forth. Unique partitions (U1, U2, U3) quantify the amount of variance in the dependant variable that is uniquely accounted for by a single predictor variable. Values can range from 0 to 1, where a value of 1 indicates all the variance is explained solely through the contribution of this variable. First order commonalities (C1, C2, C3) quantify the shared variance between two predictors, while the second order commonality (C4), describes the proportion of variance jointly explained by all three of the predictors. In the case of completely independent predictors, commonalities are null, and the sum of unique effects equals the coefficient of determination of the overall model. However, with multicollinearity, commonalities are non-null and can assume both positive and negative values. Positive values are of particular interest in this study, as they represent a synergistic association amongst predictor variables. Negative commonality values suggest the presence of suppressor variables. A suppressor variable is a predictor that removes irrelevant variance (variance not shared with the dependant variable) in another predictor, thus strengthening the relationship of that latter predictor with the dependent variable (Prunier et al., 2015; Ray-Mukherjee et al., 2014). Suppression can occur when the variable has zero or a small positive correlation with the dependent variable, but is correlated with the one or more predictor variables (Horst, 1941; Ray-Mukherjee et al., 2014; Watson, Clark, Chmielewski, & Kotov, 2013). In sum, CA allows for an improved understanding and interpretation of the influence of collinear

predictors in multiple regression, by explicitly localizing the site and amount of overlap.

The objective of the current study was to investigate the unique and common neural connectivity underlying the interface of motor, neuropsychiatric, and cognitive symptoms in PD. To achieve this objective, we applied, for the first time, regression CA to the functional connectome. We hypothesized that this analysis would reveal a significant role of the caudate nucleus, given its role in the cognitive, neuropsychiatric, and motor symptoms of Parkinson's disease (Caplan et al., 1990; Graff-Radford, Williams, Jones, & Benarroch, 2017; O'Callaghan, Bertoux, & Hornberger, 2014). However, we did not have specific expectations regarding how the variance would partition between each of the symptom domains.

2 | METHODS

2.1 | Subjects

Seventy-four non-demented PD subjects at Stages I–III of Hoehn and Yahr were diagnosed by movement disorder neurologists and met the UK brain bank criteria for idiopathic PD (Hughes, Daniel, Kilford, & Lees, 1992). Subjects were recruited from the Movement Disorder Clinic at the University of Calgary between 2014 and 2019. Exclusion criteria included neurological or severe psychiatric disease aside from idiopathic PD (including alcohol or drug dependency), dementia, inability to tolerate MRI scans, or previous deep brain stimulation surgery. With respect to psychiatric disorders, subjects have been excluded if they have a history of long-standing psychiatric disease documented in their clinical medical records by a physician.

Subjects underwent a comprehensive clinical assessment which included evaluations of cognitive, neuropsychiatric, and motor symptoms. This included a neuropsychological evaluation (Supplementary Table 1), for which we focus primarily on the Montreal Cognitive Assessment (MoCA) as a measure of global cognition, and the Unified Parkinson's Disease Rating Scale part three (UPDRS-III), which we used as a measure of global motor symptoms. The Mild Behavioral Impairment Checklist (MBI-C) was also completed for every subject and the total score was used a global measure of neuropsychiatric symptoms. The MBI-C is a 34 item instrument that is completed by a patient, close informant, or clinician (Ismail et al., 2017). It is a validated measure that captures later life onset of sustained neuropsychiatric symptoms across five domains (Hu, Patten, Fick, Smith, & Ismail, 2019; Ismail et al., 2016; Ismail et al., 2017; Mallo et al., 2018; Yoon et al., 2019). These domains include impaired drive and motivation, emotional dysregulation, impulse dyscontrol, social inappropriateness, and abnormal perception or thought content. The total MBI-C score thus represents a suitable measure of global neuropsychiatric symptoms. The entire questionnaire can be found at https://mbitest.org. Subjects also had MRI scans administered within the same week. All subjects were asked to continue taking their regular scheduled medications and thus were in the "On" state for all clinical and neuroimaging evaluations. For descriptive purposes, we classify subjects as having mild cognitive impairment (according to the

Movement Disorder Task Force Level II criteria (Litvan et al., 2012)), high MBI scores (according to a cut-off of >7.5(Mallo et al., 2018; Mallo et al., 2019; Yoon et al., 2019)), and tremor dominant, mixed, or nontremor dominant motor phenotypes, according to previous literature (Schiess, Zheng, Soukup, Bonnen, & Nauta, 2000). We also classify subjects as having minimal, mild, or moderate motor severity based on the overall UPDRS-III score (Shulman et al., 2010). Subjects provided informed consent, and the protocol was approved by the University of Calgary Research Ethics Board. Demographic information is in Table 1.

TABLE 1 Demographic details

Demographic variables	
N	74
Age	70.8 (6.0)
Gender (women)	25 (33.8%)
Education (years)	14.8 (2.8)
Disease duration (years)	5.6 (3.9)
LED (mg/day)	768.2 (381.7)
UPDRS-III	18.8 (10.5)
Minimal motor[a]	30 (40.5%)
Mild motor[b]	39 (52.7%)
Moderate motor[c]	5 (6.8%)
Tremor dominant[d]	17 (22.9%)
Nontremor dominant[e]	48 (64.8%)
Mixed[f]	9 (12.1%)
MoCA	25.1 (4.0)
Executive function (z-score)	−0.33 (0.82)
Attention (z-score)	−0.24 (0.59)
Language (z-score)	−0.12 (0.76)
Visuospatial (z-score)	−0.33 (0.92)
Memory (z-score)	−0.09 (0.83)
MCI[g]	32 (43.2%)
MBI-C (Total)	5.6 (8.3)
Drive/motivation	1.4 (2.4)
Mood/anxiety	1.8 (2.9)
Impulse dyscontrol	1.7(3.5)
Social inappropriateness	0.39 (1.3)
Perception/thought	0.30 (75)
High MBI[h]	21 (28%)
Antidepressant/anti-anxiety medication	22 (29.7%)
Cholinergic medication	2 (2.7%)
Mean motion (mm/TR)	0.21 (0.13)
Invalid volumes[i]	3.5% (8.2%)

Note: Values reported as mean (standard deviation) or number of subjects (%). a = UPDRS-III < 15; b = UPDRS-III 15–35; c = UPDRS-III >35; d = tremor/nontremor score > 1.0; e = tremor/nontremor score < 0.8; f = tremor/nontremor score 0.8–1.0; g = Movement Disorder Task Force level II criteria; h = MBI-C > 7.5; i = invalid fMRI volumes as defined in Methods: Image denoising.

2.2 | MRI acquisition and analysis

Subjects were scanned at the Seaman Family MR Center, at the University of Calgary, with a 3 T GE Discovery MR750 scanner. Sessions included a high-resolution, T1-weighted, 3D volume acquisition for anatomic localization (TR = 7.18 ms, TE = 2.25 ms, flip angle 10°, voxel size 1mm^3, 172 slices), followed by echo-planar T2*-weighted image acquisitions with BOLD contrast (TR = 2.9 sec, echo time = 30 ms; flip angle, 90°, voxel size 2.5mmx2.5mmx3mm, 48 slices, 152 volumes). Resting-state fMRI was acquired over one 7.34-minute run in a single session. During the scan, participants were presented with a black fixation cross on a white background and were instructed to keep their eyes open and look at the cross.

2.3 | Image preprocessing

Images were preprocessed using SPM 12(Friston, 2007). Functional images underwent realignment and unwarping as well as slice-time correction. The high-resolution structural images were co-registered to the mean functional image. The co-registered structural images were segmented into gray matter, white matter and cerebrospinal fluid (CSF). Functional images were nonlinearly normalized into MNI space using SPM unified normalization (Ashburner & Friston, 2005) and were spatially resampled at 2 mm^3 prior to analysis.

2.4 | Image denoising

Denoising of the functional data was performed using the MATLAB toolbox Conn (Whitfield-Gabrieli & Nieto-Castanon, 2012). Physiological and other sources of noise from the white matter and CSF signal were estimated using the aCompcor method (Behzadi, Restom, Liau, & Liu, 2007; Chai, Castanon, Ongur, & Whitfield-Gabrieli, 2012). Five principle components were extracted from eroded CSF and white matter masks and included as covariates of no-interest. To account for motion, movement parameters, and their first temporal derivative, were also included in the regression. Further quality assurance to detect outliers in motion and global signal intensity change was performed. Volumes with greater than 3 mm change of maximal composite motion, or a blood oxygen level dependent (BOLD) change >3 *SD* from the mean, were flagged as invalid and included as regressors in the first level analysis. Linear detrending, to remove signal drift, was performed. The residual BOLD time series was subjected to a high-pass filter (>0.008 Hz) prior to calculation of resting state connectivity. A full band pass filter (i.e., 0.008–0.1 Hz) was not used, as there is accumulating evidence for the relevance of higher frequencies in the resting state signal (Chen & Glover, 2015). fMRI quality control metrics were derived (mean motion (mm/TR) and number of invalid scans.

2.5 | Functional connectome

Seventy-eight regions of interest (ROI) were selected from our previous work (Lang et al., 2019). These were originally defined through high dimensional group ICA (Calhoun, Adali, Pearlson, & Pekar, 2001). ROI details can be found in Table 2. The residual BOLD time course was averaged amongst voxels within each individual ROI. As a standard measure of functional connectivity, the Pearson correlation coefficient was calculated between the average signal in each ROI, creating a 78x78 correlation matrix. To improve normality of the correlation measure, a Fisher transformation was applied. To determine the influence of the specific brain parcellation, we performed a supplementary analysis using the Brainnetome Atlas (Fan et al., 2016). This is a parcellation consisting of 246 cortical and subcortical regions based on connectional architecture.

2.6 | Commonality analysis

In order to operationalize the three symptom domains for the purpose of performing CA, we chose to use global measures of motor, cognitive, and neuropsychiatric symptoms. Motor severity was defined as the total score on the UPDRS-III, cognition was defined as the total score on the MoCA, and neuropsychiatric symptoms were defined as the total score on the MBI-C. Each of these variables were adjusted for the influence of age, gender, and medication use (levodopa equivalent dose; LED) prior to performing the commonality analysis. The variance in the functional connectome was then explained by using these three adjusted predictors (x1 = MBI-C, x2 = MoCA, and x3 = UPDRS-III) in a multiple regression model, where the dependant variable was the connectivity between each ROI (*Y(i,j)*).

$$Y(i,j) = x1 + x2 + x3$$

Significance for this overall regression model was set to *p* < .05 with a false discovery rate (FDR) correction for 78 seeds (or 246 seeds in the case of the supplementary analysis). Edges which were significantly explained by the multiple regression model were examined further with CA to determine the amount of unique and common variance of each predictor. Unique and common variance was determined by (a) performing regression of the dependent variable over all possible subsets of predictors (all possible subset regression; APS), followed by (b) applying commonality coefficient equations for each unique and common effect (Nimon, Lewis, Kane, & Haynes, 2008; Warne, 2011).

APS

$$R^2 total : Y(i,j) = x1 + x2 + x3$$

$$R^2 x1x2 : Y(i,j) = x1 + x2$$

$$R^2 x1x3 : Y(i,j) = x1 + x3$$

$$R^2 x2x3 : Y(i,j) = x2 + x3$$

TABLE 2 Region of interest (ROI) details including abbreviations used throughout the article

ROI #	Abbreviation	Anatomical region	MNI coordinates		
			x	y	z
1	L IOT (lateral)	Left inferior occipital-temporal (lateral)	−51	−51	−19
2	R MFG	Right middle frontal gyrus	36	41	28
3	R FP (lateral)	Right lateral frontal pole	47	46	−5
4	R IP	Right inferior parietal	46	−49	45
5	R FP	Right frontal pole	35	54	7
6	L FP	Left frontal pole	−36	55	6
7	L AG	Left angular gyrus	−44	−58	44
8	R IFG	Right inferior frontal gyrus	53	29	12
9	mPFC (dorsal)	Medial prefrontal cortex(dorsal)	3	31	55
10	L ins (superior)	Left insula (superior)	−40	1	10
11	R ins (superior)	Right insula (superior)	41	1	10
12	L ins (ventral)	Left insula (ventral)	−44	4	−8
13	R ins (ventral)	Right insula (ventral)	44	6	−10
14	L SMG	Left supra-marginal gyrus	−60	−29	32
15	R SMG	Right supra-marginal gyrus	62	−27	34
16	dACC	Dorsal anterior cingulate	−3	20	39
17	L MFG (anterior)	Left anterior middle frontal gyrus	−39	47	20
18	R Heschl	Right Heschls	47	−24	22
19	PCC	Posterior cingulate cortex	1	−55	33
20	ACC	Anterior cingulate cortex	0	45	4
21	L FP	Left frontal pole	−14	69	15
22	R FP	Right frontal pole	14	69	14
23	PCC	Posterior cingulate cortex	−1	53	24
24	mPFC (bilateral)	Bilateral medial prefrontal cortex	−1	52	16
25	mPFC (dorsal)	Bilateral medial prefrontal cortex (dorsal)	2	54	30
26	vmPFC	Ventromedial prefrontal cortex	2	35	−18
27	L Prc (superior)	Superior precuneus	−1	−57	54
28	mPFC (dorsal)	Bilateral medial prefrontal cortex (dorsal)	1	37	43
29	L OC (mid)	Left mid occipital	−38	−81	34
30	R OC (mid)	Right mid occipital	41	−77	36
31	L Calc	Left calcarine	−13	−59	5
32	R Calc	Right calcarine	16	−56	5
33	L Lg	Left lingual	2	−82	4
34	L FFg	Left fusiform gyrus	−24	−71	−11
35	L Cun (superior)	L Cunues (superior)	0	−81	33
36	R OC (inferior)	Right occipital (inferior)	27	−93	−2
37	L OC (inferior)	Left occipital (inferior)	−24	−95	−4
38	L OC (mid)	Left occipital (mid)	−36	−76	3
39	L OC (mid/superior)	Left occipital (mid/superior)	−35	−68	15
40	L Prc/SP	Left precuneus/superior parietal	−10	−73	45
41	R Prc	Right precuneus	13	−69	45
42	R ITC	Right inferior temporal	44	−50	−12
43	L DLPFC	Left dorsolateral prefrontal cortex	−48	8	36
44	L OC/IP	Left occipital	−27	−70	33
45	R OC/IP	Right occipital (inferior)	32	−70	32

(Continues)

TABLE 2 (Continued)

ROI #	Abbreviation	Anatomical region	MNI coordinates		
			x	y	z
46	L IP	Left inferior parietal	−42	−30	38
47	R DLPFC	Right dorsolateral prefrontal cortex	51	14	34
48	L PreC (ventral)	Left precentral gyrus (ventral)	−55	−8	30
49	R PreC (ventral)	Right precentral gyrus (ventral)	57	−5	28
50	PreC (medial)	Medial pre/post central	0	−35	65
51	R PreC	Right precentral gyrus	40	−25	60
52	SMA	Supplementary motor area	3	−13	72
53	L PreC	Left precentral gyrus	−39	−26	61
54	R STG	Right superior temporal gyrus	61	−19	5
55	L STG	Left superior temporal gyrus	−57	−24	8
56	R STG	Right superior temporal gyrus	55	−20	−5
57	R MTG/IP	Right middle temporal gyrus	57	−55	20
58	L MTG	Left middle temporal gyrus	−56	−40	−8
59	R MTG/OC	Right temporal-occipital	59	−35	−10
60	L IFG	Left inferior frontal gyrus	−50	32	1
61	R TP	Right temporal pole	35	6	−34
62	L TP	Left temporal pole	−34	6	−34
63	L TP (inferior)	Left inferior temporal pole	−42	−4	−43
64	R TP (inferior)	Right inferior temporal pole	41	−3	−45
65	OFC	Orbitofrontal cortex	−3	42	−20
66	R Cb (crus 1)	Right cerebellum crus 1	30	−71	−34
67	L Cb (crus 2)	Left cerebellum crus 2	−13	−81	−32
68	Cb (ventral)	Cerebellum (ventral)	−4	−63	−45
69	L Cb (crus 1)	Left cerebellum crus 1	−39	−58	−33
70	R Cb (dorsal)	Right cerebellum (dorsal)	29	−51	−24
71	L Cb (crus 2)	Left cerebellum (crus 2)	−8	−77	−30
72	Vermis	Vermis	−1	−59	−26
73	L Cb (ventral)	Left cerebellum (ventral)	−25	−66	−56
74	R Cb (ventral	Right cerebellum (ventrral)	25	−66	−56
75	L put	Left putamen	−26	5	0
76	R put	Right putamen	27	6	0
77	R Caud (dorsal)	Right dorsal caudate	17	6	18
78	Caud (bilateral)	Caudate (bilateral)	−1	−3	11

Note: Anatomical regions based on correspondence between the ROI coordinates and the Automated Anatomical Labelling (AAL) atlas. Region of interest (ROI) details including abbreviations used throughout the paper.

Commonality coefficient

$$U1 = R^2 total - R^2 x2x3$$

$$U2 = R^2 total - R^2 x1x3$$

$$U3 = R^2 total - R^2 x1x2$$

$$C1 = -R^2 x3 + R^2 x1x3 + R^2 x2x3 - R^2 total$$

$$C2 = -R^2 x2 + R^2 x1x2 + R^2 x2x3 - R^2 total$$

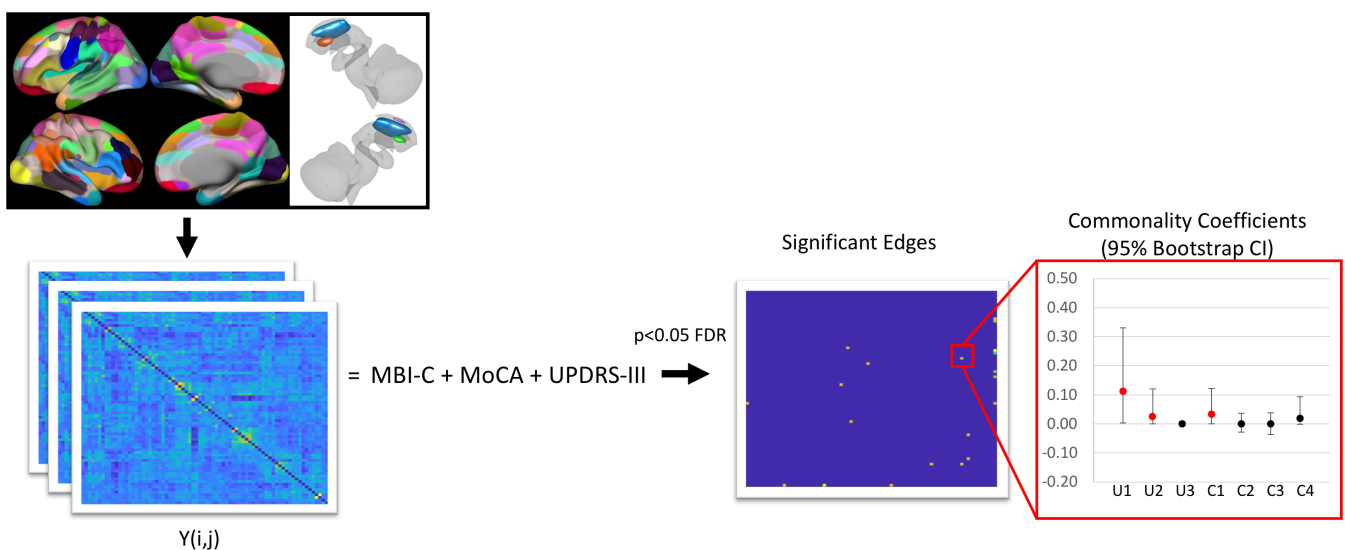$$C3 = -R^2 x1 + R^2 x1x2 + R^2 x1x3 - R^2 total$$

$$C4 = R^2 x1 + R^2 x2 + R^2 x3 - R^2 x1x2 - R^2 x1x3 - R^2 x2x3 + R^2 total$$

Commonality coefficients were calculated for each significant edge, yielding seven partition estimates corresponding to the unique and common components of variance. As is recommended in CA (Marchetti et al., 2016; Nimon et al., 2008), bootstrap estimation was used for significance testing (Wood, 2004). First, we

quantified the precision of each partition estimate by computing 95% bootstrap (bias corrected and accelerated (Diciccio & Romano, 1988)) confidence intervals (CI) on the basis of 1,000 replicates of the data using resampling with replacement. In this manner we could determine whether a specific commonality coefficient had a statistically significant contribution to the edge in question by examining the lower bound of the CI. The null hypothesis was rejected if the lower bound of the 95% CI did not contain zero. In the case of negative commonalities (suggesting a suppression effect), we considered the effect significant if the upper bound of the 95% CI was below zero. In these cases, we further examined the zero-order relationship between the relevant predictors and the edge in question to gain insight into which variable was resulting in suppression.

Secondly, we tested the statistical difference between each variance partition for every significant edge. While non-overlapping CIs represent a statistical difference, the opposite is not necessarily true (Greenland et al., 2016). Therefore, to assess if any two partitions were significantly different from each other in cases of non-overlapping CIs, for every bootstrap sample (n = 1,000), we calculated the difference between the partitions and obtained the distribution of this difference. Subsequently, we calculated the percentile based 95% CI of this difference distribution and rejected the null hypothesis (no difference between variance partition estimates) if it did not contain zero (Marchetti et al., 2016). Lastly, for descriptive purposes, the proportion of explained variance from the overall model accounted for by each partition was obtained by dividing the commonality coefficient by the total R^2. All commonality and bootstrap analyses were performed in MATLAB with a combination of custom code and the *bootci* and *bootstrp* functions. An overview of the analysis is visualized in Figure 2.

3 | RESULTS

3.1 | Demographics

Seventy-four non-demented PD subjects were included in the study. The average age was 70.8 years (57.9–81.3) and 34% were women. The average MoCA was 25.1 (standard deviation (SD) = 4.0), UPDRS-III was 18.8 (SD = 10.5) and the average total MBI-C score was 5.6 (SD = 8.3). Subjects had an average daily levodopa equivalent dose of 768.2 mg/day (SD = 381.7) and had an average disease duration of 5.6 years (SD = 3.9). Subjects had a range of cognitive and neuropsychiatric impairment, with 32 meeting formal criteria of mild cognitive impairment and 21 meeting criteria for high-MBI. Most subjects had minimal or mild motor severity (Shulman et al., 2010). Demographic details are in Table 1. The fMRI quality control metrics (mean motion and number of invalid scans) were not associated with any of the clinical scores (p > .05).
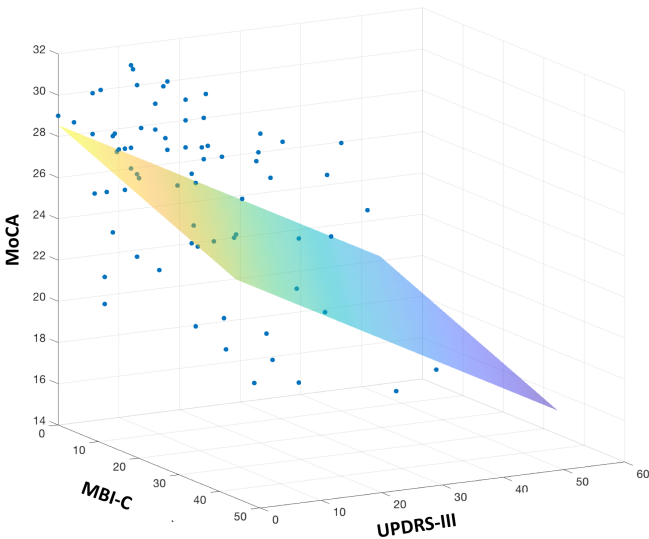
3.2 | Zero-order correlations

All three primary variables were significantly collinear with each other ($r_{\text{(MBI-C, MoCA)}}$ = −0.305, p = .008; $r_{\text{(MBI-C, UPDRS-III)}}$ = 0.287, p = .0133; $r_{\text{(MoCA, UPDRS-III)}}$ = −0.469, p = .000025) (Figure 3). These relationships remained significant after adjusting for age, gender, and LED.

3.3 | Overall model

The overall model explained a significant amount of variance in 10 edges after correction for multiple comparisons (Figure 4). The

FIGURE 2 Functional connectivity (Pearson correlation) was calculated for each pair of ROIs to create connectivity matrix for each subject. For every edge, a multiple regression was performed with connectivity as the dependent variable and MBI-C, MoCA, and UPDRS-III as the predictor variables. Significant edges were determined if the overall model had a significance of p < .05 with a FDR correction. Each resulting significant edge was then used in the commonality analysis

results of the multiple regression, including beta coefficients, are displayed in Table 3. The sign of the beta coefficient represents the direction of the relationship between connectivity and the specific symptom score. Commonality coefficients were derived for each of these edges (Figure 5). Notably 6/10 (60%) of these connections involved the caudate nucleus. Complete details of the CA from every edge are located in Supplementary Table 2.
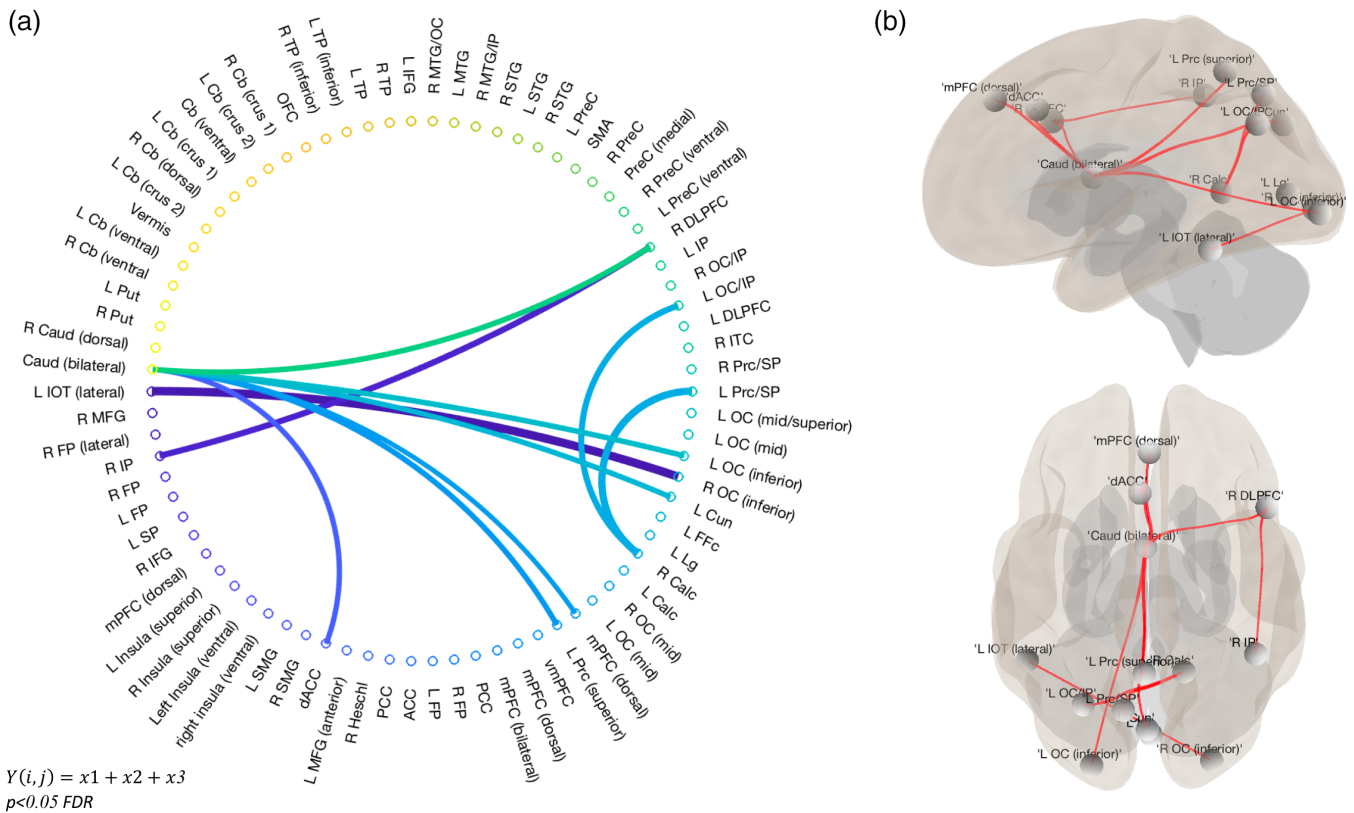
3.4 | Commonality analysis

Bootstrap 95% CIs were created to estimate the precision of the commonality coefficients. A statistically significant involvement of a particular partition in an edge was determined when the lower bound of the CI was greater than zero, or in the case of suppression, the upper bound was less than zero. With this definition, neuropsychiatric symptoms (U1; MBI-C) had a unique involvement in 9/10 edges, cognition (U2; MoCA) had a unique involvement in 5/10 edges, and motor (U3; UPDRS-III) had a unique involvement in 1 edge. Partitions were also directly compared with each other to determine if they were significantly different (Figure 6).

3.5 | Edges with a complete dominance of one partition

The explained variance in the caudate-dorsal anterior cingulate cortex (dACC) (total R^2 = .1826 (95% CI = 0.05–0.35)) and caudate-right

FIGURE 3 Global neuropsychiatric (MBI-C), cognitive (MoCA) and motor (UPDRS-III) impairment scores are significantly correlated with each other


$Y(i, j) = x1 + x2 + x3$
$p < 0.05$ FDR

FIGURE 4 The overall model identified 10 significant edges hypothesized to underlie the interface of neuropsychiatric, cognitive, and motor symptoms in PD. (a) Visualized as connectivity ring. (b) Visualized in MNI space. The list of brain region abbreviations are located in Table 2

TABLE 3   Details corresponding to the overall multiple regression model. X1 = MBI-C; X2 = MoCA; X3 = UPDRS-III

	Connection name (ROI #)	β MBI-C (*p*-value)	β MoCA (*p*-value)	β UPDRS-III (*p*-value)	Total R^2 (95% CI)
1	R IP–R DLPFC (4,47)	−0.1063 (.00009)	−0.0551 (.0570)	0.0291 (.2824)	.2150 (0.07–0.37)
2	R Calc–L Prc/SP (32,40)	0.0898 (.00002)	0.0542 (.0160)	−0.0249 (.2335)	.2577 (0.07–0.44)
3	L IOT (lateral)–R OC (inferior) (1,36)	−0.0585 (.0016)	−0.0310 (.1214)	0.0774 (.00009)	.3076 (0.12–0.54)
4	L OC/IP–R Calc (32,44)	0.0725 (.00029)	0.0514 (.0179)	−0.0225 (.2648)	.2116 (0.08–0.35)
5	Caud (bilateral)–dACC (78,16)	−0.0695 (.00026)	−0.0176 (.3843)	−0.0040 (.8346)	.1826 (0.05–0.35)
6	Caud (bilateral)–L Prc (superior) (78,27)	−0.0503 (.0028)	0.0264 (.1498)	0.0039 (.8193)	.1890 (0.04–0.42)
7	Caud (bilateral)–mPFC (dorsal) (78,28)	−0.0474 (.0085)	0.0278 (.1571)	0.0031 (.8685)	.1608 (0.04–0.27)
8	Caud (bilateral)–L Cun (78,35)	−0.0578 (.0012)	0.0228 (.2331)	0.0213 (.2382)	.1826 (0.04–0.41)
9	Caud (bilateral)–L OC (inferior) (78,37)	−0.0193 (.2932)	0.0645 (.0022)	0.0053 (.7844)	.1844 (0.03–0.33)
10	Caud (bilateral)–R DLPFC (78,47)	−0.0622 (.00014)	−0.0081 (.6409)	0.0080 (.6228)	.1916 (0.03–0.45)

Note: The sign of the beta coefficient represents the direction of the relationship between symptom score and connectivity. The list of brain region abbreviations are located in Table 2. Details corresponding to the overall multiple regression model. X1 = MBI-C; X2 = MoCA; X3 = UPDRS-III.
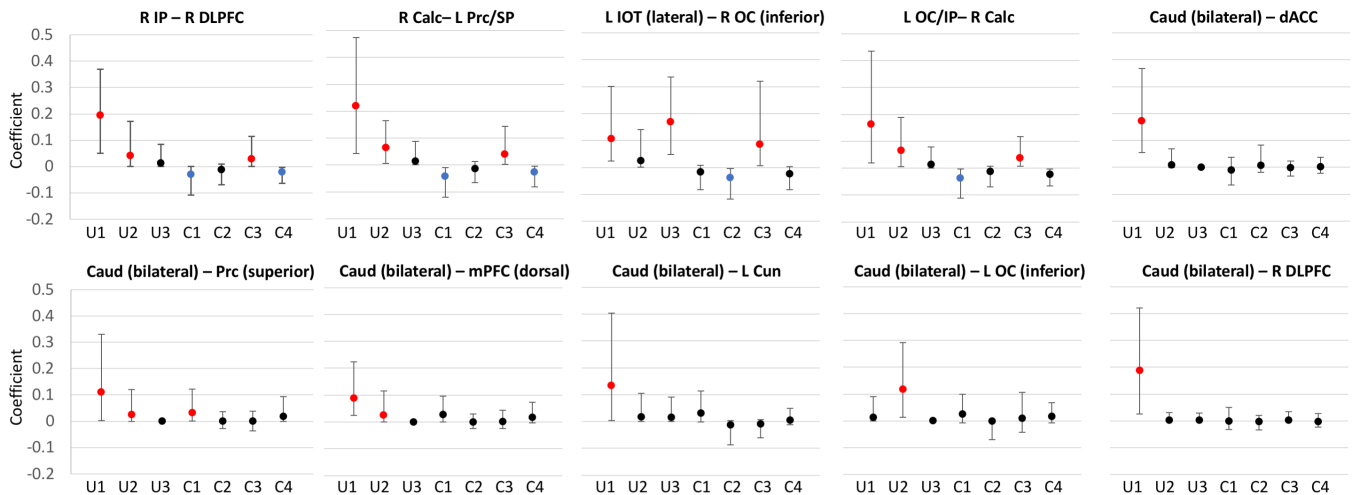
FIGURE 5   Results of the commonality analysis with 95% bootstrapped confidence intervals. Red points correspond to partitions contributing to a significant portion of explained variance (lower bound of 95% CI > 0). Blue points correspond to significantly negative coefficients (suggesting suppressor effects). U1 = unique MBI-C; U2 = unique MoCA; U3 = unique UPDRS-III; C1 = common MBI-C|MoCA; C2 = common MBI-C|UPDRS-III; C3 = common MoCA|UPDRS-III; C4 = common MBI-C|MoCA|UPDRS-III. The list of brain region abbreviations are located in Table 2

dorsolateral prefrontal cortex (DLPFC) (total R^2 = .1916 (95% CI = 0.03–0.45)) connectivity was completely dominated by the unique influence of MBI-C scores (U1 = 0.1724 (95% CI = 0.0551–0.3684) and U1 = 0.1873 (95% CI = 0.0257–0.4200), respectively), as demonstrated by the statistically significant difference between U1 and every other partition (Figure 6). No other unique coefficient showed complete dominance of the explained variability in any other edge.

partition) included caudate-left cuneus (total R^2 = .1826 (95% CI = 0.04–0.41)) with a unique contribution from MBI-C (U1 = 0.1340 (95% CI = 0.0039–0.4036)) and caudate-left inferior occipital cortex (total R^2 = .1844 (95% CI = 0.03–0.33)) with a unique contribution from MoCA (U2 = 0.1182 (95% CI = 0.0130–0.2911)). The explained variability for all other edges contained contributions from a combination of both unique and common partitions (Figure 5, Supplementary Table 2).

3.6 | Edges with a single significant partition

Other connections showing involvement of a single statistically significant partition (though not significantly different from every other

3.7 | Edges with multiple significant partitions

Motor scores were uniquely involved in one edge: the left lateral inferior occipital temporal cortex–right occipital cortex connection (total
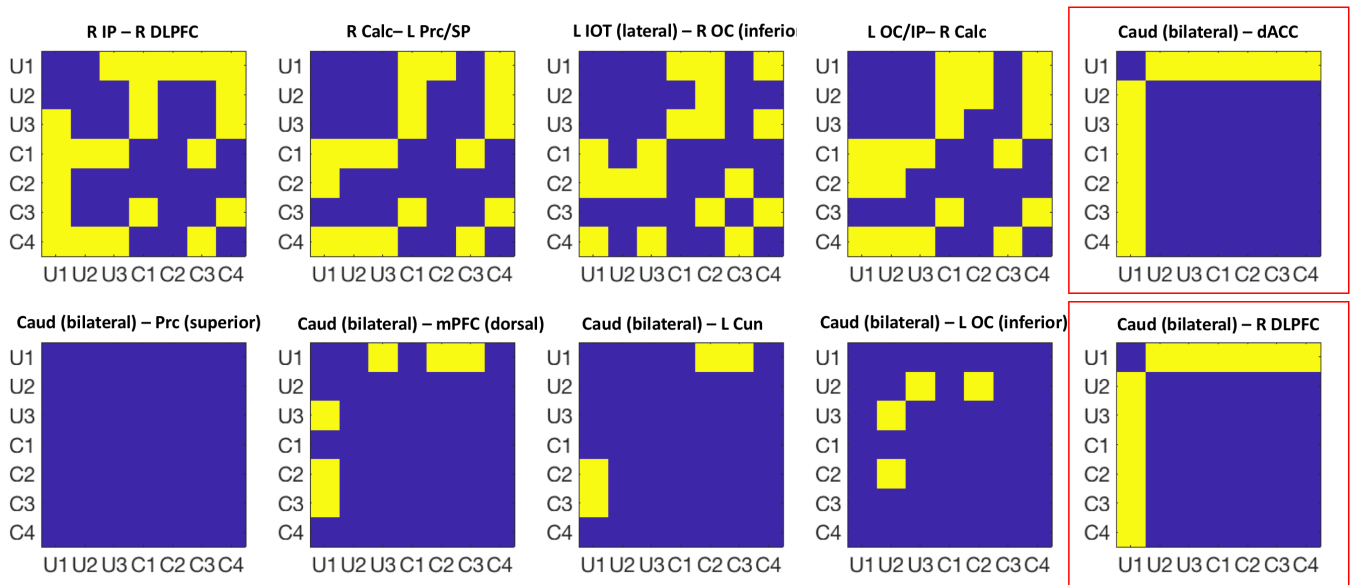
FIGURE 6 Direct pairwise comparisons between each commonality coefficient using percentile based 95% confidence intervals of the bootstrapped difference distribution. Significant comparisons determined if the 95% CI does not contain 0 (visualized in yellow). Edges which have a single partition dominate the explained variance (significantly greater than all other partitions) are outlined in red. U1 = unique MBI-C; U2 = unique MoCA; U3 = unique UPDRS-III; C1 = common MBI-C|MoCA; C2 = common MBI-C|UPDRS-III; C3 = common MoCA|UPDRS-III; C4 = common MBI-C|MoCA|UPDRS-III. The list of brain region abbreviations are located in Table 2

R^2 = .2116 (95% CI = 0.12–0.54); U3 = 0.1698 (95% CI = 0.0477–0.3355)). This edge also had a significant contribution from the unique effect of MBI-C (U1 = 0.1072 (95% CI = 0.0230–0.3007), a significant contribution from overlap between MoCA and UPDRS-III (C3 = 0.0393 (95% CI = 0.0021–0.1438), as well as a significant negative commonality (overlap between MBI-C and UPDRS-III, C2 = −0.0376 (95% CI = −0.1170 to -0.0051). Analysis of the overall regression model demonstrated significant coefficients from MBI-C (β = −.0585, p = .0016) and UPDRS-III (β = .0774, p = .00009), though univariate analysis revealed a significant relationship of only UPDRS-III (r^2 = .13, p = .0016), with no relationship of MBI-C (r^2 = .028, p = .157). This suggests a partial suppression effect of MBI-C on the UPDRS-III.

Several other edges demonstrated suppression effects. The right inferior parietal- right DLPFC connection (total R^2 = .2150 (95% CI = 0.07–0.37)) had a significant contribution from U1 (0.1939 (95% CI = 0.0502–0.3694)), U2 (0.0420 (95% CI = 0.0010–0.1719)) and C3 (0.0286 (95% CI = 0.0012–0.1151)), with significant negative input from C1 (−0.0305 (95% CI = −0.1081 to −0.0004)) and C4 (−0.0209 (95% CI = −0.0643 to −0.0030)). Analysis of the overall model demonstrated significant coefficients of the MBI-C (β = −.1063, p = .00009), with a trend of the MoCA (β = −.0551, p = .0570). The univariate analysis showed a significant relationship of MBI-C (r^2 = .156, p = .0005) but not the MoCA (r^2 = .0047, p = .562). These results suggest the unique effect of the MoCA is secondary to partial suppression of irrelevant variance in the MBI-C. The connectivity between the right calcarine–left precuneus/superior parietal region (total R^2 = .2577

(95% CI = 0.07–0.44)) showed unique contributions from U1 (0.2196 (95% CI = 0.0425–0.4746), U2 (0.0647 (95% CI = 0.0066–0.1651)), and C3 (0.0393 (95% CI = 0.0021–0.1438)), with negative input from C1(−0.0417 (95% CI = −0.1202 to −0.0096)) and C4(−0.0264 (95% CI = −0.0808 to −0.0042)). Analysis of the overall model demonstrated significant coefficients of the MBI-C (β = .0898, p = .00002) and the MoCA (β = .0552, p = .0160). The univariate analysis showed a significant relationship of MBI-C (r^2 = .105, p = .0048) but not the MoCA (r^2 = .035, p = .111). These results point to a partial suppression effect of the MoCA. Lastly, the connectivity between the left occipital cortex and the right calcarine cortex (total R^2 = .2116 (95% CI = 0.08–0.35)) showed unique contributions from U1 (0.1636 (95% CI = 0.0192–0.4346)), U2 (0.0663 (95% CI = 0.0048–0.1888)), and C3 (0.0387 (95% CI = 0.0070–0.1171)), with negative input from C1 (−0.0375 (95% CI = −0.1118 to −0.0037))and C4 (−0.0113 (95% CI = −0.0693 to −0.0078)). Analysis of the overall model demonstrated significant coefficients of the MBI-C (β = .0725, p = .00029) and the MoCA (β = .0514, p = .0179). The univariate analysis showed a significant relationship of MBI-C (r^2 = .0623, p = .032) with a trend effect of the MoCA (r^2 = .0495, p = .0567). These results also point to a partial suppression effect of the MoCA.

Connectivity between the caudate and precuneus (total R^2 = .1890 (95% CI = 0.04–0.42)) demonstrated a unique contribution from MBI-C (U1 = 0.1111 (95% CI = 0.0032–0.3310)), a unique contribution from MoCA (U2 = 0.0246 (95% CI = 0.0001–0.1206)), and a contribution from the overlap between these two symptom scores (C1 = 0.0326 (95% CI = 0.0002–0.1223)), without any suppressor effects. Lastly,

connectivity between the caudate and medial prefrontal cortex (total R^2 = .1608 (95% CI = 0.04–0.27)) also demonstrated a unique contribution from MBI-C (U1 = 0.0880 (95% CI = 0.0243–0.2241)) and a unique contribution from MoCA (U2 = 0.0245 (95% CI = 0.0001–0.1157) without any suppressor effects.

3.8 | Brainnetome atlas

The entire analysis was repeated using the 246 ROI Brainetomme Atlas (Fan et al., 2016). This was done to investigate the influence of brain parcellation on the results of the CA. The results of this analysis can be found in the Supplementary Materials (Supplementary Result I, Supplementary Tables 3-5, and Supplementary Figures 1-4).

4 | DISCUSSION

In this study, we applied CA to the functional connectome in PD to investigate the unique and common influence of neuropsychiatric, cognitive, and motor impairment on connectivity of a subnetwork lying at the interface of these symptom domains. We performed the same analysis using two brain parcellations, with different levels of resolution. We focus our discussion on the 78 ROI atlas, given this was our primary analysis. However, a discussion of the influence of brain parcellation is included for completeness.

4.1 | Overall model

The overall model assessed, for every edge in the connectome, the amount of variance which could be explained by a multiple regression model including global measures of neuropsychiatric (MBI-C), cognitive (MoCA), and motor impairment (UPDRS-III) in a group of PD subjects. Thus, we did not expect this model to capture the entire neuropsychiatric, cognitive, and motor symptomatology networks, but instead capture a subset of these networks which are at the interface of the domains. The model identified a network involving distributed cortical and subcortical regions, with a strong predominance of connections involving the caudate nucleus. The caudate nucleus has been previously identified as an interface for emotional and cognitive processing (Graff-Radford et al., 2017), and has been implicated in both cognitive and neuropsychiatric symptoms in PD (O'Callaghan et al., 2014). One study found that baseline bilateral caudate dysfunction was associated with an increased risk of developing cognitive impairment, depression, and gait problems over the course of four years (Pasquini et al., 2019). Our results support and extend this literature, placing the caudate nucleus as the primary substrate for the shared neural representation of impairment across symptom domains in PD. The subsequent CA decomposed the explained variance in this network, thereby allowing further insight in the unique and common contribution of each symptom domain.

4.2 | Commonality analysis

In total, MBI-C uniquely contributed to 90%, MoCA to 50%, and UPDRS-III to 10% of edges in the overall network. Two edges showed complete dominance of a single partition, as determined by direct pairwise comparisons using bootstrapped difference distributions. Neuropsychiatric impairment completely accounted for the explained variance in the caudate-dACC and caudate-right DLPFC connections. Normal dACC function has been linked to a range of behavioral and cognitive functions, including reward based decision making (Bush et al., 2002), fear expression (Milad et al., 2007), behavioral adaptation (Sheth et al., 2012), and cognitive valuation and control (Shenhav, Cohen, & Botvinick, 2016). Consistently, the striatal-dACC pathway has been proposed to be central to the neurobiology of apathy across disease conditions, including in PD (Le Heron, Apps, & Husain, 2018). The current results suggest that variability in this connection in PD subjects is explained primarily by the unique influence of neuropsychiatric impairment and is not related to global cognitive impairment (as measured by the MoCA). Variability in the connectivity between the caudate and the right DLPFC was also identified as being explained primarily and uniquely by neuropsychiatric impairment. The DLPFC is another region, along with the dACC and caudate, which has been implicated broadly in both cognitive and behavioral functions. Specifically, the DLPFC is involved in cognitive control (Miller & Cohen, 2001), working memory (Barbey, Koenigs, & Grafman, 2013), attention (Bishop, 2009), and goal maintenance (Wagner, Maril, Bjork, & Schacter, 2001), while also being associated with depression (Koenigs & Grafman, 2009), anxiety (Schmidt, Khalid, Loukas, & Tubbs, 2018), psychosis (Colibazzi et al., 2016) and addiction (Goldstein & Volkow, 2011). Moreover, functional connectivity of the DLPFC to striatum predicts treatment response of depression to transcranial magnetic stimulation (Avissar et al., 2017), suggesting a direct role of this pathway in depressive symptomatology. In PD, frontostriatal connectivity has been implicated in deficits of executive functioning (Owen, 2004), often manifesting as a dysexecutive cognitive syndrome (Kehagia, Barker, & Robbins, 2012; Williams-Gray et al., 2009). Our results suggest that the variability in connectivity of the caudate and right DLPFC can be accounted primarily by the unique effect of global neuropsychiatric impairment, as measured by the MBI-C. Speculatively, a potential clinical implication of these findings is that the MBI-C is a more sensitive measure of early neurodegenerative changes in frontostriatal "executive function" circuits as compared to the MoCA. MBI is thought to be a good predictor of cognitive decline and dementia in non-PD subjects (Creese et al., 2019; Taragano et al., 2009; Taragano et al., 2018), and our results suggest that this might also be true for PD. However, we also found evidence that the MoCA captures at least some variability in frontostriatal circuitry. Specifically, we found a unique influence of both the MBI-C and the MoCA on caudate-dorsal medial prefrontal cortex connectivity, suggesting that both symptom domains are reflected depending on the circuit interrogated.

Nevertheless, consistent with the interpretation that MBI-C better reflects variability in executive functioning circuitry, we found

explained variability in the connectivity between the right DLPFC and right inferior parietal lobe was almost completely accounted for by the unique influence of MBI-C. The right inferior parietal lobe has complex, multidimensional functions, with a hypothesized role in both maintaining attentive control on current task goals, as well as in responding to salient new information in the environment (Singh-Curry & Husain, 2009). In particular, the right inferior parietal lobe allows for the flexible reconfiguration of behavior between these two modes (Singh-Curry & Husain, 2009). Overall, our results suggest that in PD subjects, the complex cognitive and behavioral control functions of the right DLPFC-right inferior parietal circuit is captured to a greater degree by MBI-C scores than by the MoCA. Indeed, the explanatory power of the MBI-C was improved by the addition of the MoCA in the model, despite the MoCA having no relationship with the connectivity of this edge. In this case the MoCA acted as a partial suppressor, removing irrelevant variance from the MBI-C. However, this relationship is complex, as the overlap between the MoCA and the UPDRS-III also contributed to a small portion of the explained variance in this connection.

This same pattern was seen in the connectivity between the right calcarine cortex and both the left precuneus/superior parietal region and left occipital/inferior parietal region. Specifically, most of the explained variability in connectivity was accounted for by the unique effect of the MBI-C (with a suppression effect of the MoCA) with a smaller portion of variance explained by the overlap of motor and cognitive symptoms. Meanwhile, connectivity between the left inferior occipital-temporal region and the right inferior occipital region was accounted for primarily through the unique influence of UPDRS-III, with some variability explained by the unique influence of MBI-C and the overlap between UPDRS-III and MoCA. However, a portion of the unique effect of the MBI-C can be attributed to the partial suppression of irrelevant variance in the UPDRS-III, thereby improving the latter's explanatory power. Overall, our results suggest that posterior cortical connectivity reflects an interplay of neuropsychiatric, motor and cognitive impairment, with some connections primarily reflecting neuropsychiatric symptoms (right calcarine-left precuneus/superior parietal, right calcarine-left occipital/inferior parietal) some cognitive (caudate-left inferior occipital), and others motor symptoms (left inferior occipital temporal- right occipital). Along with these unique influences, this posterior cortical connectivity reflects, at least partly, a common substrate of cognitive and motor impairment. Consistent with our findings, structural and functional abnormalities in posterior cortical regions have previously been shown to contribute to motor (Bohnen, Minoshima, Giordani, Frey, & Kuhl, 1999; Lord, Archibald, Mosimann, Burn, & Rochester, 2012; Tessitore et al., 2012), cognitive (Dubbelink et al., 2014; Hanganu et al., 2014) and neuropsychiatric symptoms (Pagonabarraga et al., 2014; Shine et al., 2015). It is possible these pathways represent part of the network underlying complex phenomena such as freezing of gait, which is associated with impairment across symptom domains (Ehgoetz Martens et al., 2018), and likely involves dysfunction in visual and cognitive networks (Tessitore et al., 2012).

Lastly, variability in the caudate-precuneus connection reflected the overlap between MBI-C and MoCA, suggesting a shared neural substrate for global cognitive and neuropsychiatric symptoms. Caudate-precuneus connectivity has previously been shown to be related to cognitive impairment (Anderkova, Barton, & Rektorova, 2017), while precuneus atrophy has been related to various neuropsychiatric symptoms such as depression (Liang et al., 2016) and apathy (Shin et al., 2017).

4.3 | Brain parcellation

The results from the 246 ROI atlas suggest that the choice of brain parcellation has a substantial effect on the overall model and subsequent CA. First, consistent with the 78 ROI atlas, the caudate nucleus was a hub in the network at the interface of the symptom domains. With the improved resolution of the Brainnetome Atlas, it was found that the right dorsal caudate nucleus was the primary subregion of the caudate involved. Also consistent with the main analysis, it was found that connectivity between the caudate (right dorsal) and the cingulate gyrus (caudodorsal area 24) was completely explained by the MBI-C. Additionally, the connectivity of the right dorsal caudate to the parietal lobe appeared to reflect a common substrate of impairment in each symptom domain, given that the overlap of the MBI-C, MoCA, and UPDRS-III (C4) significantly contributed to explaining variability between the right dorsal caudate and four ROIs clustered in the superior and inferior parietal region.

Inconsistent with the original analysis, we found that the UPDRS-III played a larger role in explaining the variance in connectivity. For example, the explained variability in connectivity between the left postcentral gyrus–right dorsal insular gyrus and the right cingulate gyrus (caudal area 23)–left insular gyrus was completely accounted for by the unique influence of UPDRS-III. The unique influence of UPDRS-III was also the only significant partition in several other edges, including the right premotor thalamus–right precentral gyrus area 4, and two other edges involving the insula. These results suggest that the reason the UPDRS-III was not reflected to major degree in the 78 ROI analysis was a function of the resolution of the brain parcellation (rather than, for example, the normalization of motor related connectivity by continued dopaminergic medication use (Bell et al., 2014; Szewczyk- et al., 2014; Wu et al., 2009)). While we did not observe as much symptom related connectivity in the occipital cortices using the 246 ROI atlas, we did observe relationships between various symptom domains and the connectivity of subregions of the insula (associated primarily with the unique effect of UPDRS-III and the overlap of UPDRS-III and MoCA) and the amygdala (associated primarily with the unique effect of MBI-C), which have previously been widely implicated across symptom domains in Parkinson's disease (Christopher, Koshimori, Lang, Criaud, & Strafella, 2014; Criaud et al., 2016).

Overall, it is clear that the choice of brain parcellation can influence the specific results of this type of analysis, though many consistencies remain. The choice of what brain parcellation to use is an

active issue in functional connectomics (Arslan et al., 2018; de Reus & Van den Heuvel, 2013), and indeed there may not be a single best choice (Arslan et al., 2018; Salehi et al., 2020). Different cortical parcellations represent the brain at different levels of spatial resolution, and the results must be interpreted within this context. We would recommend that authors employing CA of the functional connectome report the results from several different cortical parcellations and report on the consistencies (and inconsistencies).

4.4 | Limitations

Several limitations are present in the current investigation. For example, we are unable to determine the influence of medication, as all our subjects were treated and continued on dopaminergic therapy during the study. However, by adjusting for the influence of LED on each predictor variable, we can conclude the results we report are independent from medication dose differences between subjects. We also cannot determine which effects we observe are pathological vs which are compensatory in nature. Likewise, 29.7% of subjects were taking antidepressant/anti-anxiety medication (Supplementary Table 6). These medications can result in confounding effects on functional connectivity, though these effects are variable (Gudayol-Ferré, Peró-Cebollero, González-Garrido, & Guàrdia-Olmos, 2015) and may have complex relationships with disease severity in PD (Borchert et al., 2019).

Related to the overall model specification, the symptom domains have been represented by general clinical scores, for which many of the complexities and subtleties of the actual symptomatology are missed. This is necessitated by the fact that the complexity of the analysis increases substantially with increasing predictor variables. For every predictor variable (x) added to the overall model, the number of commonalities is equal to $2^x - 1$. Therefore, to facilitate the interpretation and computation of commonalities, we limited the overall regression model to three predictor variables. It is also important to acknowledge that our population consisted of a heterogenous group of PD subjects, and thus the results represent an average effect across motor, cognitive, and neuropsychiatric subtypes. More insight into subtype specific connectivity profiles could be gained by refining the patient population. Finally, commonalities are specific to the specified model, and the addition or deletion of predictors may change the uniqueness attributed to some of the variables.

5 | CONCLUSION

In conclusion, this manuscript represents the first application of CA to the functional connectome. We demonstrate that this method can determine the amount of variance in the connectome that is unique and shared amongst motor, neuropsychiatric, and cognitive symptoms, thereby improving our ability to interpret the data while gaining novel insight into the pathophysiology of PD. Amongst these results, several key features emerge. Specifically, consistent with previous literature, we find evidence that the caudate nucleus is a major hub in the network underlying the interface of these symptom domains. We show that in PD, caudate-dACC, caudate-right DLPFC, and right DLPFC-right inferior parietal connectivity is driven primarily by neuropsychiatric symptoms, measured by the MBI-C. This has potentially important clinical implications, suggesting the MBI-C might be a more sensitive screening tool for detecting early pathological connectivity changes in these executive functioning circuits as compared to the MoCA. We also show that posterior cortical connectivity represents a complex interplay of neuropsychiatric, cognitive, and motor impairment. The commonality analysis provides a detailed interrogation of this circuitry, allowing for insight into the unique and common representation of symptom domains. We show that while the results can be influenced by the resolution of the brain parcellation, many consistencies remain. Further work with refined patient subgroups could complement and enhance these findings. Finally, this analytical method could be adapted to other patient groups with correlated symptom domains.

CONFLICT OF INTEREST

There are no conflicts of interest to declare for any author.

DATA AVAILABILITY STATEMENT

Data availability Commonality coefficient functions, demographic data, connectivity matrices, and the brain parcellation image file used in this manuscript are available at https://github.com/slang092/Commonality. The Brainnetome Atlas (Fan et al., 2016) is available from https://atlas.brainnetome.org/index.html. The remaining data and code that support the finding of this manuscript are available from the first or the corresponding author, upon reasonable request.

ORCID

Stefan Lang https://orcid.org/0000-0001-8960-0640
Oury Monchi https://orcid.org/0000-0003-2148-5409

REFERENCES

Aarsland, D., Marsh, L., & Schrag, A. (2009). Neuropsychiatric symptoms in Parkinson's disease. *Movement Disorders*, 24, 2175–2186. https://doi.org/10.1002/mds.22589

Aarsland, D., Taylor, J.-P., & Weintraub, D. (2014). Psychiatric issues in cognitive impairment. *Movement Disorders*, 29, 651–662. https://doi.org/10.1002/mds.25873

Anderkova, L., Barton, M., & Rektorova, I. (2017). Striato-cortical connections in Parkinson's and Alzheimer's diseases: Relation to cognition. *Movement Disorders*, 32, 917–922. https://doi.org/10.1002/mds.26956

Arslan, S., Ktena, S. I., Makropoulos, A., Robinson, E. C., Rueckert, D., & Parisot, S. (2018). Human brain mapping: A systematic comparison of parcellation methods for the human cerebral cortex. *NeuroImage*, *170*, 5–30. http://www.sciencedirect.com/science/article/pii/S1053811917303026

Ashburner, J., & Friston, K. J. (2005). Unified segmentation. *NeuroImage*, *26*, 839–851. http://www.sciencedirect.com/science/article/pii/S1053811905001102

Avissar, M., Powell, F., Ilieva, I., Respino, M., Gunning, F. M., Liston, C., & Dubin, M. J. (2017). Functional connectivity of the left DLPFC to striatum predicts treatment response of depression to TMS. *Brain Stimulation*, *10*, 919–925. http://www.sciencedirect.com/science/article/pii/S1935861X17308422

Barbey, A. K., Koenigs, M., & Grafman, J. (2013). Dorsolateral prefrontal contributions to human working memory. *Cortex*, *49*, 1195–1205. https://doi.org/10.1016/j.cortex.2012.05.022

Behzadi, Y., Restom, K., Liau, J., & Liu, T. T. (2007). A component based noise correction method (CompCor) for BOLD and perfusion based fMRI. *NeuroImage*, *37*, 90–101.

Bell, P. T., Gilat, M., O'Callaghan, C., Copland, D. A., Frank, M. J., Lewis, S. J. G., & Shine, J. M. (2014). Dopaminergic basis for impairments in functional connectivity across subdivisions of the striatum in Parkinson's disease. *Human Brain Mapping*, *36*, 1278–1291.

Bishop, S. J. (2009). Trait anxiety and impoverished prefrontal control of attention. *Nature Neuroscience*, *12*, 92–98. https://doi.org/10.1038/nn.2242

Biundo, R., Weis, L., & Antonini, A. (2016). Cognitive decline in Parkinson's disease: The complex picture. *NPJ Parkinson's Disease*, *2*, 16018. http://www.nature.com/articles/npjparkd201618

Bohnen, N. I., Minoshima, S., Giordani, B., Frey, K. A., & Kuhl, D. E. (1999). Motor correlates of occipital glucose hypometabolism in Parkinson's disease without dementia. *Neurology*, *52*, 541.

Borchert, R. J., Rittman, T., Rae, C. L., Passamonti, L., Jones, S. P., Vatansever, D., ... Rowe, J. B. (2019). Atomoxetine and citalopram alter brain network organization in Parkinson's disease. *Brain Communications*, *1*, fcz013. https://pubmed.ncbi.nlm.nih.gov/31886460

Burn, D. J., Rowan, E. N., Allan, L. M., Molloy, S., & Mckeith, I. G. (2006). Motor subtype and cognitive decline in Parkinson's disease, Parkinson's disease with dementia, and dementia with Lewy bodies. *Journal of Neurology, Neurosurgery, and Psychiatry*, *77*, 585–589.

Burn, D. J., Landau, S., Hindle, J. V., Samuel, M., Wilson, K. C., Hurt, C. S., ... Group for the P-PS. (2012). Parkinson's disease motor subtypes and mood. *Movement Disorders*, *27*, 379–386. https://doi.org/10.1002/mds.24041

Bush, G., Vogt, B. A., Holmes, J., Dale, A. M., Greve, D., Jenike, M. A., & Rosen, B. R. (2002). Dorsal anterior cingulate cortex: A role in reward-based decision making. *Proceedings of the National Academy of Sciences of the United States of America*, *99*, 523–528. http://www.pnas.org/content/99/1/523.abstract

Calhoun, V. D., Adali, T., Pearlson, G. D., & Pekar, J. J. (2001). A method for making group inferences from functional MRI data using independent component analysis. *Human Brain Mapping*, *151*, 140–151.

Caplan, L. R., Schmahmann, J. D., Kase, C. S., Feldmann, E., Baquis, G., Greenberg, J. P., ... Hier, D. B. (1990). Caudate Infarcts. *Archives of Neurology*, *47*, 133–143. https://doi.org/10.1001/archneur.1990.00530020029011

Castrioto, A., Thobois, S., Carnicella, S., Maillet, A., & Krack, P. (2016). Emotional manifestations of PD: Neurobiological basis. *Movement Disorders*, *31*, 1103–1113.

Chai, X. J., Castanon, A. N., Ongur, D., & Whitfield-Gabrieli, S. (2012). Anticorrelations in resting state networks without global signal regression. *NeuroImage*, *59*, 1420–1428.

Chen, J. E., & Glover, G. H. (2015). BOLD fractional contribution to resting-state functional connectivity above 0.1Hz. *NeuroImage*, *107*, 207–218. http://www.sciencedirect.com/science/article/pii/S1053811914010040

Christopher, L., Koshimori, Y., Lang, A. E., Criaud, M., & Strafella, A. P. (2014). Uncovering the role of the insula in non-motor symptoms of Parkinson's disease. *Brain*, *137*, 2143–2154.

Colibazzi, T., Horga, G., Wang, Z., Huo, Y., Corcoran, C., Klahr, K., ... Peterson, B. S. (2016). Neural dysfunction in cognitive control circuits in persons at clinical high-risk for psychosis. *Neuropsychopharmacology*, *41*, 1241–1250. https://doi.org/10.1038/npp.2015.273

Creese, B., Brooker, H., Ismail, Z., Wesnes, K. A., Hampshire, A., Khan, Z., ... Ballard, C. (2019). Mild behavioral impairment as a marker of cognitive decline in cognitively Normal older adults. *The American Journal of Geriatric Psychiatry*, *27*, 823–834.

Criaud, M., Christopher, L., Boulinguez, P., Ballanger, B., Lang, A. E., Cho, S. S., ... Strafella, A. P. (2016). Contribution of insula in Parkinson's disease: A quantitative meta-analysis study. *Human Brain Mapping*, *37*, 1375–1392.

Diciccio, T. J., & Romano, J. P. (1988). A review of bootstrap confidence intervals. *Journal of the Royal Statistical Society, Series B*, *50*, 338–354. https://doi.org/10.1111/j.2517-6161.1988.tb01732.x

Dubbelink, K. T. E. O., Schoonheim, M. M., Deijen, J. B., Twisk, J. W. R., Barkhof, F., & Berendse, H. W. (2014). Functional connectivity and cognitive decline over 3 years in Parkinson disease. *Neurology*, *83*, 2046–2053.

Ehgoetz Martens, K. A., Hall, J. M., Georgiades, M. J., Gilat, M., Walton, C. C., Matar, E., ... Shine, J. M. (2018). The functional network signature of heterogeneity in freezing of gait. *Brain*, *141*, 1145–1160. https://doi.org/10.1093/brain/awy019

Fan, L., Li, H., Zhuo, J., Zhang, Y., Wang, J., Chen, L., ... Jiang, T. (2016). The human Brainnetome atlas: A new brain atlas based on connectional architecture. *Cerebral Cortex*, *26*, 3508–3526. https://doi.org/10.1093/cercor/bhw157

Filippi, M., Sarasso, E., & Agosta, F. (2019). Resting-state functional MRI in Parkinsonian syndromes. *Movement Disorders Clinical Practice*, *6*, 104–117. https://doi.org/10.1002/mdc3.12730

Friston, K. (2007). In K. Friston, J. Ashburner, S. Kiebel, T. Nichols, & B. T. William (Eds.), *Statistical parametric mapping: The analysis of functional brain images*. London: Academic Press.

Gao, L., & Wu, T. (2016). The study of brain functional connectivity in Parkinson's disease. *Translational Neurodegeneration*, *5*, 18. https://doi.org/10.1186/s40035-016-0066-0

Goldstein, R. Z., & Volkow, N. D. (2011). Dysfunction of the prefrontal cortex in addiction: Neuroimaging findings and clinical implications. *Nature Reviews. Neuroscience*, *12*, 652–669. https://www.ncbi.nlm.nih.gov/pubmed/22011681

Graff-Radford, J., Williams, L., Jones, D. T., & Benarroch, E. E. (2017). Caudate nucleus as a component of networks controlling behavior. *Neurology*, *89*, 2192–2197. https://www.ncbi.nlm.nih.gov/pubmed/29070661

Greenland, S., Senn, S. J., Rothman, K. J., Carlin, J. B., Poole, C., Goodman, S. N., & Altman, D. G. (2016). Statistical tests, P values, confidence intervals, and power: A guide to misinterpretations. *European Journal of Epidemiology*, *31*, 337–350. https://www.ncbi.nlm.nih.gov/pubmed/27209009

Gudayol-Ferré, E., Peró-Cebollero, M., González-Garrido, A. A., & Guàrdia-Olmos, J. (2015). Changes in brain connectivity related to the treatment of depression measured through fMRI: A systematic review. *Frontiers in Human Neuroscience*, *9*, 582.

Hanganu, A., Bedetti, C., Degroot, C., Mejia-Constain, B., Lafontaine, A. L., Soland, V., ... Monchi, O. (2014). Mild cognitive impairment is linked with faster rate of cortical thinning in patients with Parkinson's disease longitudinally. *Brain*, *137*, 1120–1129.

Le Heron, C., Apps, M. A. J., & Husain, M. (2018). The anatomy of apathy: A neurocognitive framework for amotivated behaviour. *Neuropsychologia*, *118*, 54–67.

Horst, P. (1941). The role of predictor variables which are independent of the criterion. *Social Science Research Council Bulletin*, 48, 431–436.

Hu, M. T. M., Szewczyk-Królikowski, K., Tomlinson, P., Nithi, K., Rolinski, M., Murray, C., ... Ben-Shlomo, Y. (2014). Predictors of cognitive impairment in an early stage Parkinson's disease cohort. *Movement Disorders*, 29, 351–359. https://doi.org/10.1002/mds.25748

Hu, S., Patten, S. B., Fick, G., Smith, E. E., & Ismail, Z. (2019). Validation of the mild behavioral checklist (MBI-C) in a clinic-based sample. *Alzheimer's and Dementia: The Journal of the Alzheimer's Association*, 15, P365. https://doi.org/10.1016/j.jalz.2019.06.872

Hughes, A. J., Daniel, S. E., Kilford, L., & Lees, A. J. (1992). Accuracy of clinical diagnosis of idiopathic Parkinson's disease: A clinico-pathological study of 100 cases. *Journal of Neurology, Neurosurgery, and Psychiatry*, 55, 181–184.

Ismail, Z., Agüera-Ortiz, L., Brodaty, H., Cieslak, A., Cummings, J., Fischer, C. E., ... NPSPIA of the IS of to AAR and T (NPS-P of ISTAART). (2017). The mild behavioral impairment checklist (MBI-C): A rating scale for neuropsychiatric symptoms in pre-dementia populations. *Journal of Alzheimer's Disease*, 56, 929–938.

Ismail, Z., Smith, E. E., Geda, Y., Sultzer, D., Brodaty, H., Smith, G., ... Lyketsos, C. G. (2016). Neuropsychiatric symptoms as early manifestations of emergent dementia: Provisional diagnostic criteria for mild behavioral impairment. *Alzheimer's and Dementia: The Journal of the Alzheimer's Association*, 12, 195–202. http://www.sciencedirect.com/science/article/pii/S1552526015002150

Jankovic, J. (2008). Parkinson's disease: Clinical features and diagnosis. *Journal of Neurology, Neurosurgery, and Psychiatry*, 79, 368–376.

Janvin, C. C., Larsen, J. P., Aarsland, D., & Hugdahl, K. (2006). Subtypes of mild cognitive impairment in Parkinson's disease: Progression to dementia. *Movement Disorders*, 21, 1343–1349.

Kehagia, A. A., Barker, R. A., & Robbins, T. W. (2012). Cognitive impairment in Parkinson's disease: The dual syndrome hypothesis. *Neurodegenerative Diseases*, 11, 79–92.

Koenigs, M., & Grafman, J. (2009). The functional neuroanatomy of depression: Distinct roles for ventromedial and dorsolateral prefrontal cortex. *Behavioural Brain Research*, 201, 239–243.

Kulisevsky, J., Pagonabarraga, J., Pascual-Sedano, B., García-Sánchez, C., Gironell, A., & Trapecio Study Group. (2008). Prevalence and correlates of neuropsychiatric symptoms in Parkinson's disease without dementia. *Movement Disorders*, 23, 1889–1896. https://doi.org/10.1002/mds.22246

Lang, S., Hanganu, A., Gan, L. S., Kibreab, M., Auclair-Ouellet, N., Alrazi, T., ... Monchi, O. (2019). Network basis of the dysexecutive and posterior cortical cognitive profiles in Parkinson's disease. *Movement Disorders*, 34, 893–902. https://doi.org/10.1002/mds.27674

Lee, H. M., & Koh, S.-B. (2015). Many faces of Parkinson's disease: Non-motor symptoms of Parkinson's disease. *Journal of Movement Disorders*, 8, 92–97.

Liang, P., Deshpande, G., Zhao, S., Liu, J., Hu, X., & Li, K. (2016). Altered directional connectivity between emotion network and motor network in Parkinson's disease with depression. *Medicine (Baltimore)*, 95, e4222.

Litvan, I., Goldman, J. G., Tröster, A. I., Ben, A., Weintraub, D., Petersen, R. C., ... Williams-gray, C. H. (2012). Diangostic criteria for mild cognitive impairment in Parkinson's disease:Movement Disorder Society task force guidelines. *Movement Disorders*, 27, 349–356.

Lord, S., Archibald, N., Mosimann, U., Burn, D., & Rochester, L. (2012). Dorsal rather than ventral visual pathways discriminate freezing status in Parkinson's disease. *Parkinsonism & Related Disorders*, 18, 1094–1096.

Mallo, S. C., Ismail, Z., Pereiro, A. X., Facal, D., Lojo-Seoane, C., Campos-Magdaleno, M., & Juncos-Rabadán, O. (2018). Assessing mild behavioral impairment with the mild behavioral impairment-checklist in people with mild cognitive impairment. *Journal of Alzheimer's Disease*, 66, 83–95.

Mallo, S. C., Ismail, Z., Pereiro, A. X., Facal, D., Lojo-Seoane, C., Campos-Magdaleno, M., & Juncos-Rabadán, O. (2019). Assessing mild behavioral impairment with the mild behavioral impairment checklist in people with subjective cognitive decline. *International Psychogeriatrics*, 31, 231–239.

Marchetti, I., Loeys, T., Alloy, L. B., & Koster, E. H. W. (2016). Unveiling the structure of cognitive vulnerability for depression: Specificity and overlap. *PLoS One*, 11, 1–16. https://doi.org/10.1371/journal.pone.0168612

Milad, M. R., Quirk, G. J., Pitman, R. K., Orr, S. P., Fischl, B., & Rauch, S. L. (2007). A role for the human dorsal anterior cingulate cortex in fear expression. *Biological Psychiatry*, 62, 1191–1194.

Miller, E. K., & Cohen, J. D. (2001). An integrative theory of prefrontal cortex function. *Annual Review of Neuroscience*, 24, 167–202. https://doi.org/10.1146/annurev.neuro.24.1.167

Monastero, R., Di Fiore, P., Ventimiglia, G. D., Camarda, R., & Camarda, C. (2013). The neuropsychiatric profile of Parkinson's disease subjects with and without mild cognitive impairment. *Journal of Neural Transmission*, 120, 607–611. https://doi.org/10.1007/s00702-013-0988-y

Nimon, K., Lewis, M., Kane, R., & Haynes, R. M. (2008). An R package to compute commonality coefficients in the multiple regression case: An introduction to the package and a practical example. *Behavior Research Methods*, 40, 457–466.

Nimon, K., & Reio, T. G. (2011). Regression commonality analysis: A technique for quantitative theory building. *Human Resource Development Review*, 10, 329–340.

O'Callaghan, C., Bertoux, M., & Hornberger, M. (2014). Beyond and below the cortex: The contribution of striatal dysfunction to cognition and behaviour in neurodegeneration. *Journal of Neurology, Neurosurgery, and Psychiatry*, 85, 371–378.

Owen, A. M. (2004). Cognitive dysfunction in Parkinson's disease: The role of Frontostriatal circuitry. *Neuroscientist*, 10, 525–537. https://doi.org/10.1177/1073858404266776

Pagonabarraga, J., Soriano-Mas, C., Llebaria, G., López-Solà, M., Pujol, J., & Kulisevsky, J. (2014). Neural correlates of minor hallucinations in non-demented patients with Parkinson's disease. *Parkinsonism & Related Disorders*, 20, 290–296. https://doi.org/10.1016/j.parkreldis.2013.11.017

Pasquini, J., Durcan, R., Wiblin, L., Gersel Stokholm, M., Rochester, L., Brooks, D. J., ... Pavese, N. (2019). Clinical implications of early caudate dysfunction in Parkinson's disease. *Journal of Neurology, Neurosurgery, and Psychiatry*, 90, 1098–1104.

Poewe, W. (2008). Non-motor symptoms in Parkinson's disease. *European Journal of Neurology*, 15, 14–20. https://doi.org/10.1111/j.1468-1331.2008.02056.x

Prodoehl, J., Burciu, R. G., & Vaillancourt, D. E. (2014). Resting state functional magnetic resonance imaging in Parkinson's disease. *Current Neurology and Neuroscience Reports*, 14, 448.

Prunier, J. G., Colyn, M., Legendre, X., Nimon, K. F., & Flamand, M. C. (2015). Multicollinearity in spatial genetics: Separating the wheat from the chaff using commonality analyses. *Molecular Ecology*, 24, 263–283.

Ray-Mukherjee, J., Nimon, K., Mukherjee, S., Morris, D. W., Slotow, R., & Hamer, M. (2014). Using commonality analysis in multiple regressions: A tool to decompose regression effects in the face of multicollinearity. *Methods in Ecology and Evolution*, 5, 320–328.

de Reus, M., & Van den Heuvel, M. P. (2013). The parcellation based connectome: Limitations and extensions. *NeuroImage*, 80, 397–404.

Riedel, O., Klotsche, J., Spottke, A., Deuschl, G., Förstl, H., Henn, F., ... Wittchen, H.-U. (2010). Frequency of dementia, depression, and other neuropsychiatric symptoms in 1,449 outpatients with Parkinson's disease. *Journal of Neurology*, 257, 1073–1082. https://doi.org/10.1007/s00415-010-5465-z

Salehi, M., Greene, A. S., Karbasi, A., Shen, X., Scheinost, D., & Constable, R. T. (2020). There is no single functional atlas even for a single individual: Functional parcel definitions change with task. *NeuroImage*, 208, 116366.

Schapira, A. H. V., Chaudhuri, K. R., & Jenner, P. (2017). Non-motor features of Parkinson disease. *Nature Reviews Neuroscience*, 18, 435–450. https://doi.org/10.1038/nrn.2017.62

Schiess, M. C., Zheng, H., Soukup, V. M., Bonnen, J. G., & Nauta, H. J. W. (2000). Parkinson's disease subtypes: Clinical classification and ventricular cerebrospinal fluid analysis. *Parkinsonism & Related Disorders*, 6, 69–76.

Schmidt, C. K., Khalid, S., Loukas, M., & Tubbs, R. S. (2018). Neuroanatomy of anxiety: A brief review. *Cureus*, 10, e2055–e2055.

Schneider, J. S., Sendek, S., & Yang, C. (2015). Relationship between motor symptoms, cognition, and demographic characteristics in treated mild/moderate Parkinson's disease. *PLoS One*, 10, e0123231.

Shenhav, A., Cohen, J. D., & Botvinick, M. M. (2016). Dorsal anterior cingulate cortex and the value of control. *Nature Neuroscience*, 19, 1286–1291. https://doi.org/10.1038/nn.4384

Sheth, S. A., Mian, M. K., Patel, S. R., Asaad, W. F., Williams, Z. M., Dougherty, D. D., … Eskandar, E. N. (2012). Human dorsal anterior cingulate cortex neurons mediate ongoing behavioural adaptation. *Nature*, 488, 218–221. https://doi.org/10.1038/nature11239

Shin, J. H., Shin, S. A., Lee, J.-Y., Nam, H., Lim, J.-S., & Kim, Y. K. (2017). Precuneus degeneration and isolated apathy in patients with Parkinson's disease. *Neuroscience Letters*, 653, 250–257.

Shine, J. M., Muller, A. J., O'Callaghan, C., Hornberger, M., Halliday, G. M., & Lewis, S. J. G. (2015). Abnormal connectivity between the default mode and the visual system underlies the manifestation of visual hallucinations in Parkinson's disease: A task-based fMRI study. *NPJ Parkinsons's Disease*, 1, 15003. https://doi.org/10.1038/npjparkd.2015.3

Shulman, L. M., Gruber-Baldini, A. L., Anderson, K. E., Fishman, P. S., Reich, S. G., & Weiner, W. J. (2010). The clinically important difference on the unified Parkinson's disease rating scale. *Archives of Neurology*, 67, 64–70. https://doi.org/10.1001/archneurol.2009.295

Singh-Curry, V., & Husain, M. (2009). The functional role of the inferior parietal lobe in the dorsal and ventral stream dichotomy. *Neuropsychologia*, 47, 1434–1448.

Solla, P., Cannas, A., Floris, G. L., Orofino, G., Costantino, E., Boi, A., … Marrosu, F. (2011). Behavioral, neuropsychiatric and cognitive disorders in Parkinson's disease patients with and without motor complications. *Progress in Neuro-psychopharmacology & Biological Psychiatry*, 35, 1009–1013.

Svenningsson, P., Westman, E., Ballard, C., & Aarsland, D. (2012). Cognitive impairment in patients with Parkinson's disease: Diagnosis, biomarkers, and treatment. *Lancet Neurology*, 11, 697–707.

Szewczyk-, K., RAL, M., Rolinski, M., Duff, E., Zamboni, G., & Mackay, C. E. (2014). Functional connectivity in the basal ganglia network differentiates PD patients from controls. *Neurology*, 83, 208–214.

Tahmasian, M., Eickhoff, S. B., Giehl, K., Schwartz, F., Herz, D. M., Drzezga, A., … Eickhoff, C. R. (2017). Resting-state functional reorganization in Parkinson's disease: An activation likelihood estimation meta-analysis. *Cortex*, 92, 119–138.

Taragano, F. E., Allegri, R. F., Heisecke, S., Martelli, M., Feldman, M., Sanchez, V., … Dillon, C. (2018). Risk of conversion to dementia in a mild behavioral impairment group compared to a psychiatric group and to a mild cognitive impairment group. *Journal of Alzheimer's Disease*, 62, 227–238.

Taragano, F. E., Allegri, R. F., Krupitzki, H., Sarasola, D. R., Serrano, C. M., Loñ, L., & Lyketsos, C. G. (2009). Mild behavioral impairment and risk of dementia: A prospective cohort study of 358 patients. *The Journal of Clinical Psychiatry*, 70, 584–592.

Tessitore, A., Amboni, M., Esposito, F., Russo, A., Picillo, M., Marcuccio, L., … Barone, P. (2012). Resting-state brain connectivity in patients with Parkinson's disease and freezing of gait. *Parkinsonism & Related Disorders*, 18, 781–787.

Valli, M., Mihaescu, A., & Strafella, A. P. (2019). Imaging behavioural complications of Parkinson's disease. *Brain Imaging and Behavior*, 13, 323–332.

Wagner, A. D., Maril, A., Bjork, R. A., & Schacter, D. L. (2001). Prefrontal contributions to executive control: fMRI evidence for functional distinctions within lateral prefrontal cortex. *NeuroImage*, 14, 1337–1347.

Warne, R. T. (2011). Beyond multiple regression: Using commonality analysis to better understand r2 results. *The Gifted Child Quarterly*, 55, 313–318.

Watson, D., Clark, L. A., Chmielewski, M., & Kotov, R. (2013). The value of suppressor effects in explicating the construct validity of symptom measures. *Psychological Assessment*, 25, 929–941.

Wen, M. C., Chan, L. L., Tan, L. C. S., & Tan, E. K. (2016). Depression, anxiety, and apathy in Parkinson's disease: Insights from neuroimaging studies. *European Journal of Neurology*, 23, 1001–1019.

Whitfield-Gabrieli, S., & Nieto-Castanon, A. (2012). Conn: A functional connectivity toolbox for correlated and anticorrelated brain networks. *Brain Connectivity*, 2, 125–141.

Williams-Gray, C. H., Evans, J. R., Goris, A., Foltynie, T., Ban, M., Robbins, T. W., … Barker, R. A. (2009). The distinct cognitive syndromes of Parkinson's disease: 5 year follow-up of the CamPaIGN cohort. *Brain*, 132, 2958–2969.

Wood, M. (2004). Statistical inference using bootstrap confidence intervals. *Significance*, 1, 180–182. https://doi.org/10.1111/j.1740-9713.2004.00067.x

Wu, T., Wang, L., Chen, Y., Zhao, C., Li, K., & Chan, P. (2009). Changes of functional connectivity of the motor network in the resting state in Parkinson's disease. *Neuroscience Letters*, 460, 6–10.

Yarnall, A. J., Breen, D. P., Duncan, G. W., Khoo, T. K., Coleman, S. Y., Firbank, M. J., … Burn, D. J. (2014). Characterizing mild cognitive impairment in incident Parkinson disease: The ICICLE-PD study. *Neurology*, 82, 308–316.

Yoon, E. J., Ismail, Z., Hanganu, A., Kibreab, M., Hammer, T., Cheetham, J., … Monchi, O. (2019). Mild behavioral impairment is linked to worse cognition and brain atrophy in Parkinson disease. *Neurology*, 93, e766–e777.

Zientek, L. R., & Thompson, B. (2006). Commonality analysis: Partitioning variance to facilitate better understanding of data. *Journal of Early Intervention*, 28, 299–307.

SUPPORTING INFORMATION

Additional supporting information may be found online in the Supporting Information section at the end of this article.